International Conference on Space Optics—ICSO 2018

Chania, Greece

9–12 October 2018

Edited by Zoran Sodnik, Nikos Karafolas, and Bruno Cugny

Measuring, modeling and removing optical straylight from Venμs Super Spectral Camera images

P. Gamet

S. Fourest

T. Sprecher

E. Hillairet

esa icso proceedings cnes

International Conference on Space Optics — ICSO 2018, edited by Zoran Sodnik, Nikos Karafolas, Bruno Cugny, Proc. of SPIE Vol. 11180, 111804F · © 2018 ESA and CNES · CCC code: 0277-786X/18/$18 · doi: 10.1117/12.2536078

Measuring, modeling and removing optical straylight from Venμs Super Spectral Camera images

Philippe Gamet[a], Sébastien Fourest[a], Tuvia Sprecher[b], Emmanuel Hillairet[c]
[a]Centre National d'Etudes Spatiales (CNES), 18 avenue Edouard Belin, 31401 TOULOUSE Cedex 9, France; [b]ELOP ltd., advanced technology park Kiryat Weizmann, P.O.B. 1165 Rehovot 76111, ISRAEL; [c]Magellium Toulouse, Parc technologique du Canal, 24, rue Hermès, 31521 Ramonville Saint-Agne, France

ABSTRACT

The Venμs Super Spectral Camera suffers from high level of optical straylight. The probable causes of this defect will be discussed. Two types of straylight are observed: local ghost is caused by scattering of optical surfaces of the instrument, and multiple reflexions between detector and filter or filter window, or lenses. Cross-talk ghost is constituted of light going through the filter of one band, and impacting another band on the same detector. It is caused by multiple reflexions between detectors and filter.

The optical set-up used to evaluate the straylight patterns will be presented, and then, the approach used to characterize and model the observed phenomena will be detailed:

Local straylight model is computed as a global system MTF that includes the local straylight. The assumption is made that the phenomenon can be modeled by a convolution, and that it is slowly variable within the instrument field of view. Cross-talk straylight is modeled from a pinhole, used to extract the impulsive response of the cross-talk. The cross-talk pattern is observed through the ghost generated by a saturated input signal. The cross-talk signals for all contributing bands of the same tri-detector are substracted from the image of each band.

The performances of the correction model are presented: on the ground over test pattern images, and then in-flight during the image quality commissioning phase, over specific targets: moon, sand/water transitions.

Keywords: optical straylight, MTF, diffraction, pinhole, cross-talk, correction model, the Moon

1. INTRODUCTION

1.1 Venμs mission

Venμs (Vegetation and Environment on a New Micro Satellite) is an Earth observation demonstration mission launched August 1st, 2017 developed in cooperation between FRANCE and ISRAEL in the framework of the European GMES (Global Monitoring for Environment and Security) Program [1]. The main goal of the Venμs scientific mission is to acquire data over land in order to improve the understanding and the modeling of land surface and vegetation processes, and to develop new applications such as water balance, crop yield and carbon fluxes assessments [2].

The main payload for Venμs is the Venμs Super Spectral Camera (VSSC). In terms of spectral resolution, the VSSC is composed of 12 spectral bands in visible and NIR spectrum (420 to 910nm, BW from 15nm to 40nm), including a 620nm band which is duplicated (B5 and B6) for stereoscopic capability.

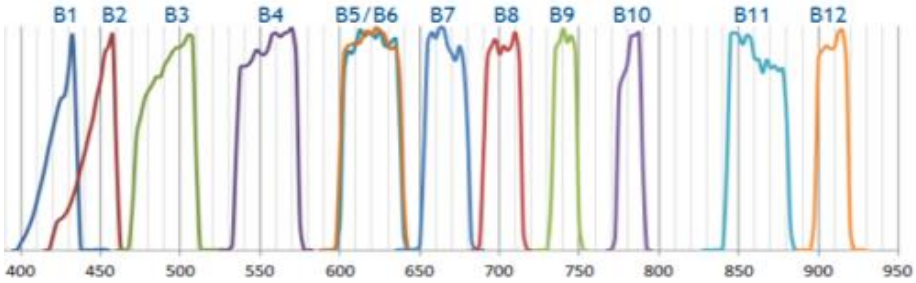

Figure 1. The spectral responses of Venμs 12 spectral bands B1 to B12

Venμs combines high spatial resolution (the native ground sampling distance is 5.3 meters) and high temporal resolution (2-day repeat orbit). 110 scientific sites have been selected on the Earth, each of them is observed close to 10:30 local time every 2 days with a constant view angle (up to 30 degrees w.r.t. nadir) during the whole mission duration (2.5 years at least). The processed products are generated with resolution varying from 5.3m to 10m (depending on the level of processing).

1.2 Venμs products levels

The image products levels provided by the ground segment are:

- Inventory and Level 0 products: raw acquisitions at native spatial resolution
- Level 1A: radiometric corrections applied (including equalization and straylight correction)
- Level 1: geolocated ortho-rectified products with top-of-atmosphere reflectance at 5 meters resolution, including clouds identification
- Level 2: ortho-image of ground reflectance, after atmospheric correction at 10 meters resolution, providing an improved cloud and shadow mask
- Level 3: multi-temporal synthesis of ortho-images: ground reflectance, 10-day composite of level 2 products at 10 meters resolution.

2. CAMERA DESIGN

The VSSC payload is a super-spectral camera, specified by CNES and manufactured by ELOP (subsidiary of Elbit systems, Israel). The optics is a 1750 mm focal length F/7 Ritchey-Chrétien type telescope, corrector optimized for tele-centricity and spectral band uniformity in the field-of-view. It includes light-weighted primary and secondary mirrors, a composite material tube structure, straylight baffles and a sunshield. Camera focus was optimized for 720km S/C altitude, and no refocus mechanism is included. Tight cleanliness requirements were specified in order to minimize stray light: mirror roughness 5Å, particle contamination <300 ppm.

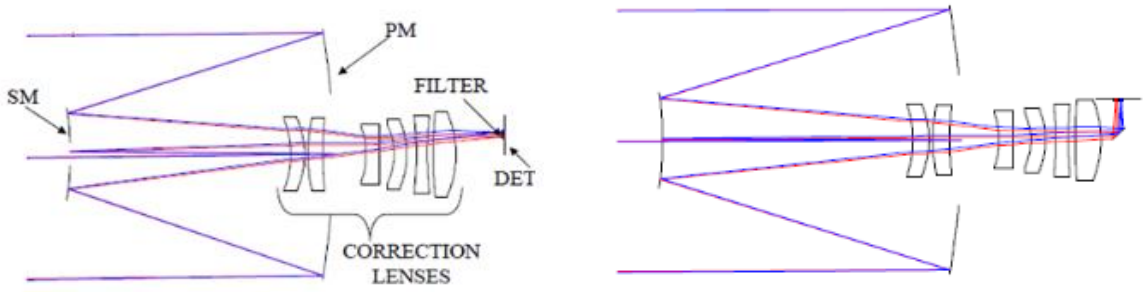

Figure 2. VSSC objective optical lay-out: unfolded channels (left) and folded channels (right)

The VSSC Detector Focal Plane Assembly (DFPA) includes folding mirrors, wideband spectral absorbing filters and precisely machined band apertures to limit straylight, as well as the detector units.
The 4 detector units each are tri-band 5200 pixel TDI (Time Delay Integration) CCD detectors with narrow band interference filters attached to the inside of each unit's Detector Spectral Window (DSW).

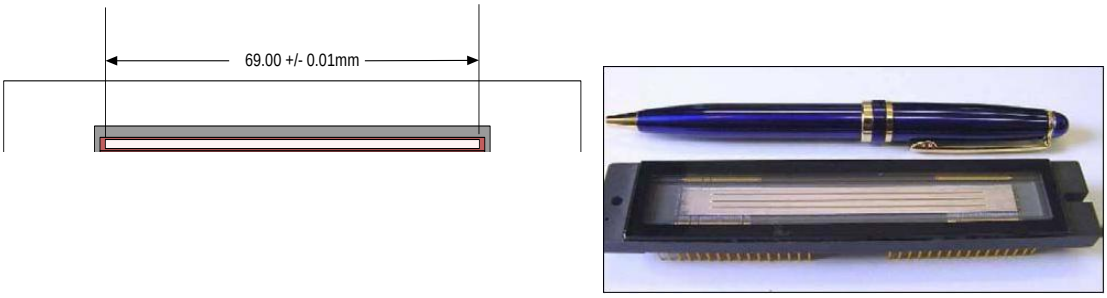

Figure 3. Detector Unit (left) and Detector Spectral Window (DSW) (right)

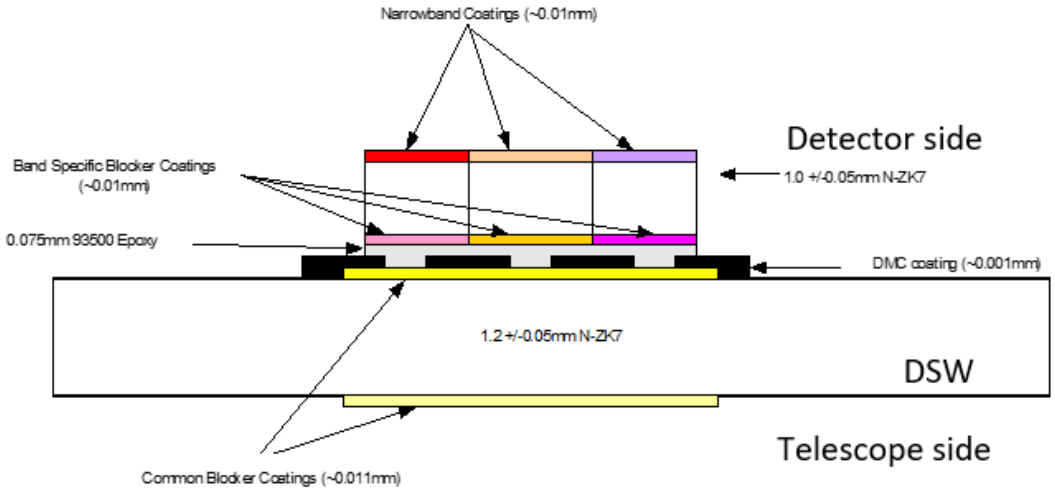

Figure 4. Design of Detector Spectral Window (DSW)

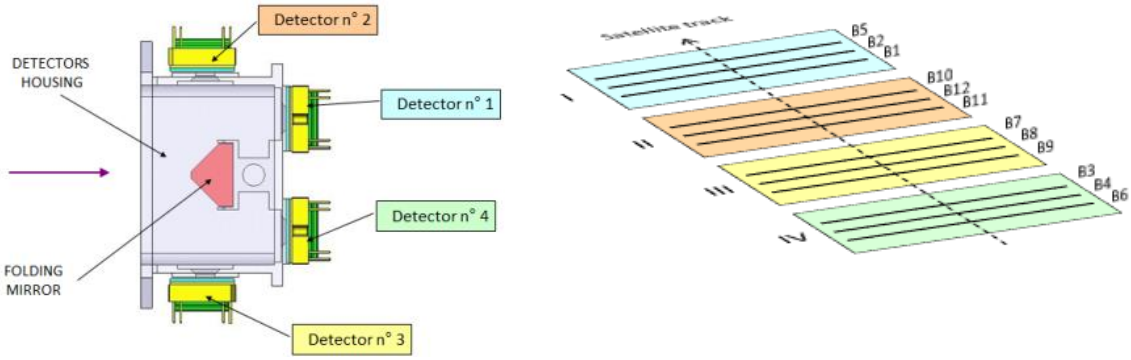

Figure 5. Layout of DFPA (left), projection of the push-broom type acquisition on the ground (right)

Along track spacecraft velocity provides the scanning mechanism for the 12 parallel detector bands in the focal plane to acquire images in pushbroom mode.

3. VENUS STRAYLIGHT AS MEASURED ON GROUND AND IN FLIGHT

3.1 Observed types of straylight

Four different types of straylight were observed in the images and are listed and illustrated below. Note that for the sample images from the IOT campaign shown below the image dynamics have been adapted to accentuate the straylight phenomena.

A Local Ghost (type 1 straylight, or SL1) is observed around bright areas, and affects particularly sharp transitions between bright and dark targets.

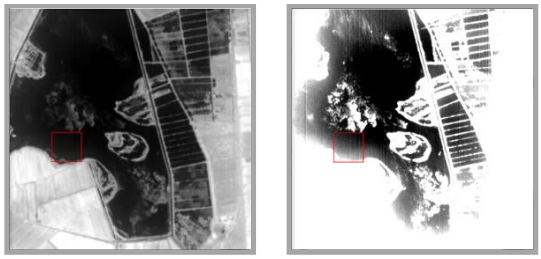

Figure 6. SL1 straylight on B12 (Maccarese sea shore, Italy)

A Crosstalk Ghost (type 2 straylight, or SL2) is observed as a nearly focused ghost image at a certain distance from a bright target. The distance corresponds to the inter-detector distance in the focal plane, while the amplitude of the ghost is dependent on the radiance level received in the source band.

Figure 7. SL2 ghosts on a Moon image in B3 (crosstalk ghosts from both B4 and B6 are visible)

Other types of ghost patterns are observable specifically in bands B12 (SL3) and other bands (SL4), on the ground and in flight. These ghosts are of very low amplitude (within noise level), and almost undetectable on terrestrial images, with B1 the most affected band. In B12 the ghost measured amplitudes are about 1% of the signal.

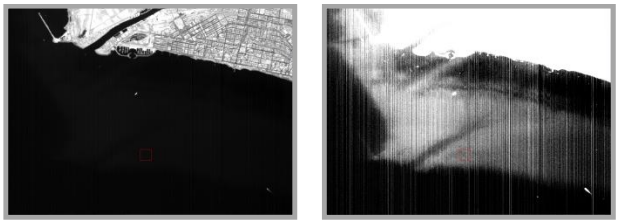

Figure 8. SL3 straylight pattern on B12 (Maccarese sea shore, Italy)

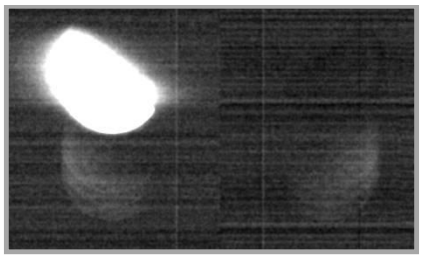

Figure 9. SL4 straylight patterns on moon image (B4)

A strategy to reduce the impact of SL1 and SL2 straylight has been developed. It includes characterizing the straylight on the ground before launch, modeling both types of straylight and implementing a correction algorithm in the operational Level-1 processing chain as will be described below.
No correction has been studied for the other types of straylight, as their impact on the mission is very limited.

3.2 Classification of the straylight phenomena

Description of the observed four types of straylight:

- A Local Ghost (Local Straylight or SL1) results from reflection and scattering of the incoming light by optical surfaces: telescope mirrors, correction lenses, folding mirrors, spectral filters, and/or detector window. Visualizing this straylight using a point source, the typical straylight pattern would be a circular spot surrounding the target image, whose intensity is low and dependent on the size of the illuminated area. A dissymmetry of the ghost with respect to the target image may be expected, due to the angle of incidence of the beam, especially when the illuminated area is at edge of the image swath. However practically point sources could not be used to characterize SL1, as will be discussed below.

- An additional source for SL1 will be comprised of light at the spectral edges of the narrowband filter's pass-band, reflected up from the detector-die, and then reflected back by the interference type filter to the detector-die. Assuming specular reflection, the angles are very small and the ghost will be located very close to, or even slightly overlapping, the legitimate image.
- A Crosstalk Ghost (SL2) results from light passing through the spectral filter of one detector band, followed by multiple reflections between detector-die surface and the narrowband spectral filters, finally impacting on another band within the same detector unit. This might be especially severe if light is reflected from the detector die at unexpected large reflection angles, thus enabling the light after few reflections to reach neighbour bands. This straylight is typically not localized with the image spot. On different missions, different shapes are possible: rings as observed on POLDER instruments, ghosts, and/or continuous background.
- The third type of straylight (SL3) as observed in the B12 band might possibly be caused by an imperfection in the optical surface at the top of the folding mirror facing detector D2.
- The fourth type of straylight (SL4) observed only in moon images could have an electronic origin as this type of straylight shows up as mirror images in both left-half and right-half of the detector band.

3.3 Taking a closer look at Crosstalk Ghosts between bands

Results from straylight characterization measurement data showed crosstalk ghosting between bands much more severe than expected. The following sketch shows the Crosstalk Ghost mechanism:

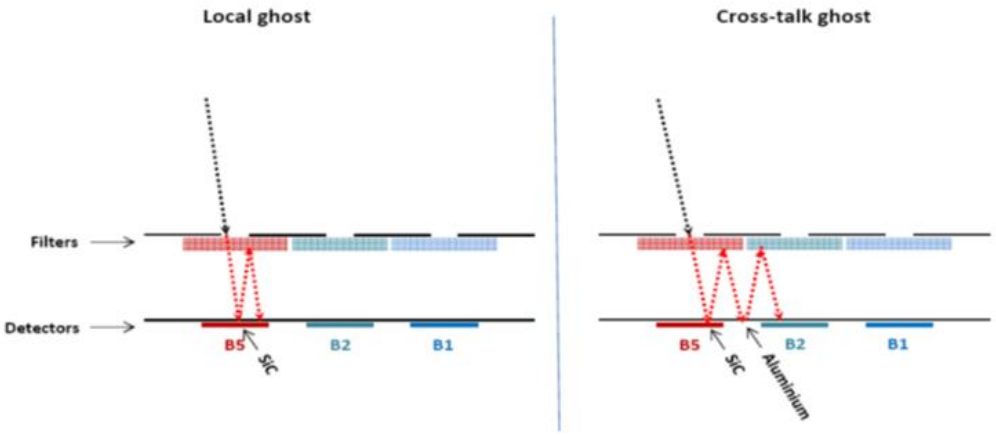

Figure 10. Local Ghost (left) and Crosstalk Ghost mechanism

The Crosstalk Ghosting between bands might be due to a combination of several factors:

- Low manufacturing yields were encountered while coating the narrowband filters onto the outside surface of the DSW, requiring a change of the DSW original design, instead manufacturing the filters as narrow spectral filter strips assembled as a "butcher-block" glued onto the inside of the DSW. This resulted in the interference filter surfaces, which are reflective for out-of-band wavelengths, to be significantly closer to the detector-die surface, thus worsening possible multiple reflections.

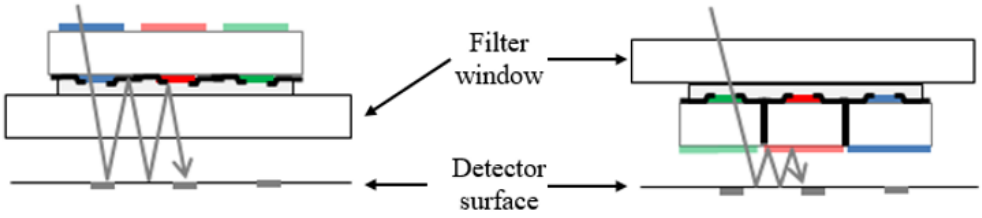

Figure 11. Initial DSW design (left): the filters are outside the detector cavity. Final DSW design (right): no absorbing coating is facing the detector

- The crosstalk phenomenon is possibly magnified by the regular spaced structures etched in the detector-die surface acting as a "grating" and generating reflections in non-specular reflection angles.

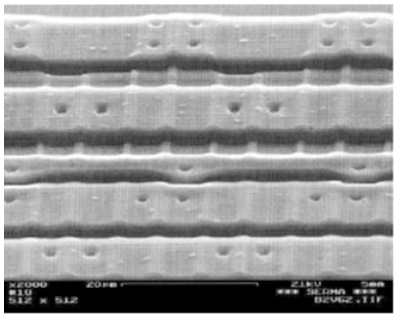

Figure 12. Structures etched in the detector silicon

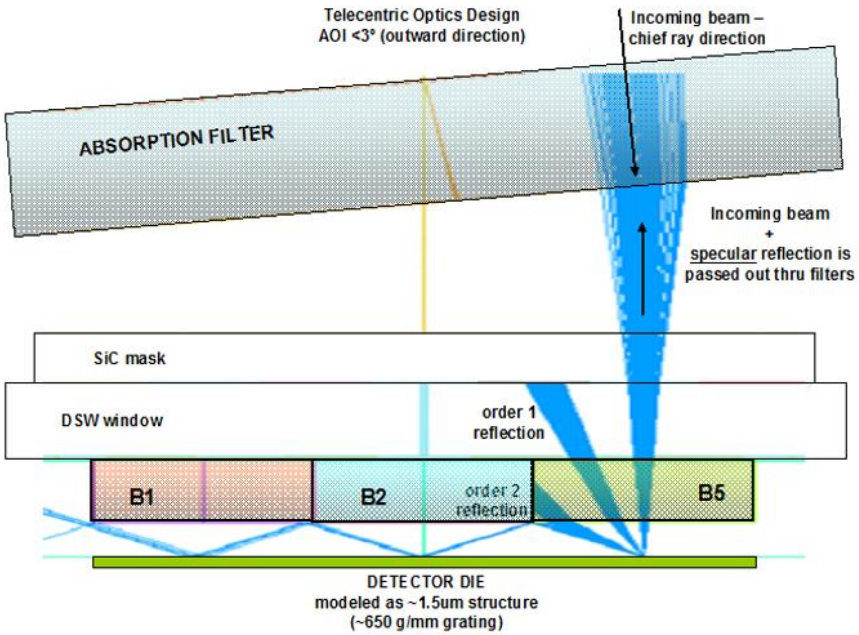

Figure 13. Non-specular reflections from the detector-die, acting as a grating

4. GROUND MEASUREMENT CAMPAIGN: SET-UP AND DATA COLLECTION

4.1 Setup for 2-D Image Data Collection

The objective for the straylight data collection campaign is to achieve acquisition of a large number of 2-D images of specified targets. In order to enable image acquisition under circumstances closely representing the camera operating in space, the VSSC was mounted into a Thermal Vacuum Chamber (TVAC), facing a Newton type 5500mm collimator, which is an integral part of the TVAC.

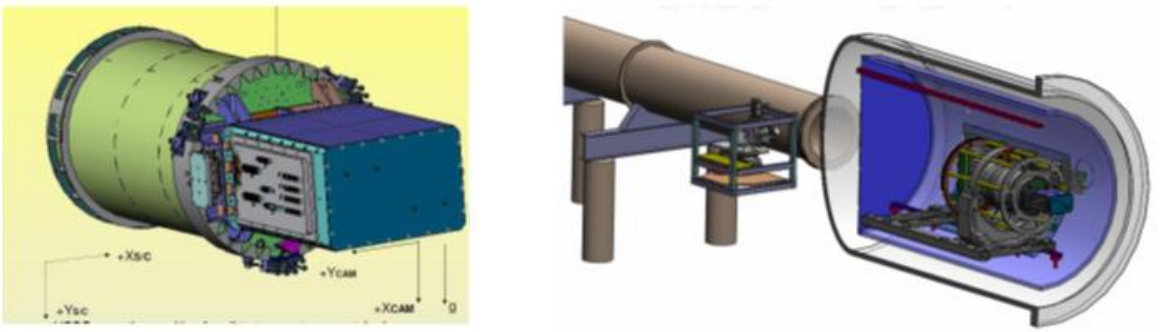

Figure 14. VSSC with scan direction downwards (left), VSSC on 2-axis gimbals in the TVAC facing collimator (right)

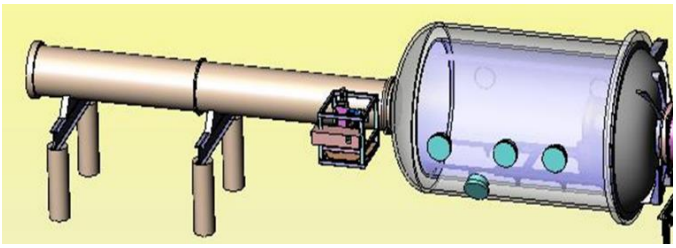

Figure 15. VSSC insertion into TVAC (left), TVAC with integral collimator (right)

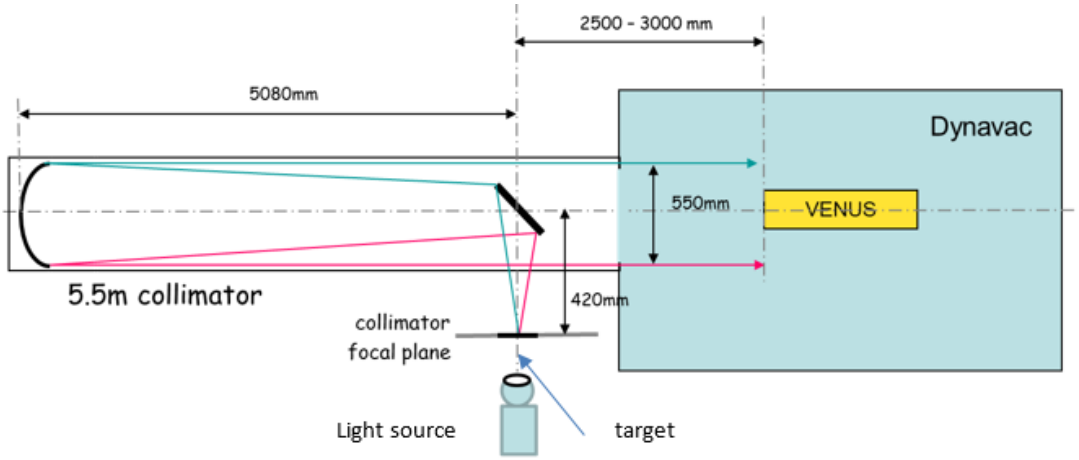

Figure 16. VSSC versus collimator optics setup

In order to acquire 2-D images with the VSSC, which is essentially a line-camera operating in pushbroom image acquisition mode, relative motion is required between the camera and the target. As it is not practical to move the camera, a target plate in the collimator focal plane is mounted on a set of remote controlled very high step resolution linear translators. This arrangement allows adjusting the target position in the collimator focal plane horizontally (to be projected onto the desired pixel area of the VSSC), as well as moving the target with constant velocity in vertical direction (camera scan direction). In order to capture well focused 2-D images it is crucial that the direction of motion of the target projection in the VSSC focal plane shall be identical to the detector's TDI direction, and the target projection scan velocity in the VSSC focal plane be exactly compatible to the commanded VSSC line-rate.

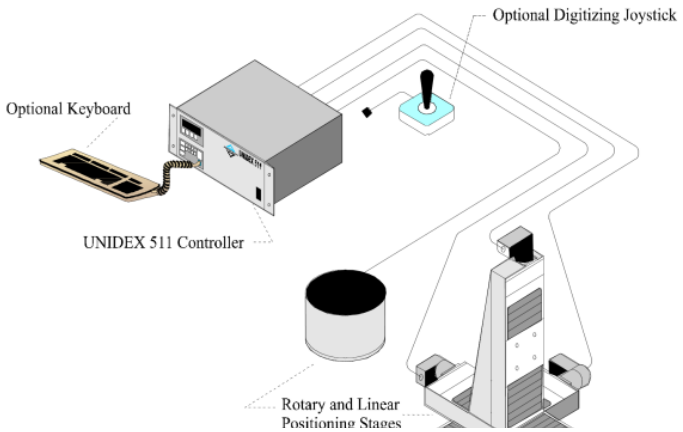

Figure 17. Remote controlled Linear Translators

The target plate is manufactured by means of laser cutting from a 0.1mm thick stainless-steel plate and incorporates a number of specified pinholes and rectangular targets, as well as a central area with targets designed to be used for focusing procedures of the target plate versus the VSSC.

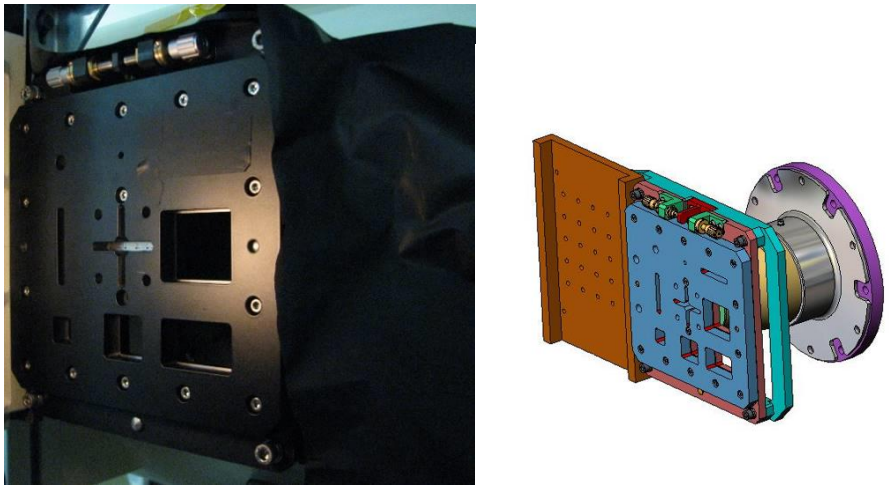

Figure 18. Target plate holder design (left) and implementation (right)

The target plate is held flat between two thicker parts of the target plate-holder, holes in the target plate holder allow back-illumination of the target plate and projection via the collimator towards the VSSC. This design guarantees correct focusing of all the pinholes, based on a focusing procedure performed using the focusing targets in the center of the target plate. The target plate holder was improved relative to the above illustrations by bevelling all edges of the holes and blackening all parts of the holder, as well as covering up all holes not currently used in order to prevent straylight being introduced by the measurement setup.

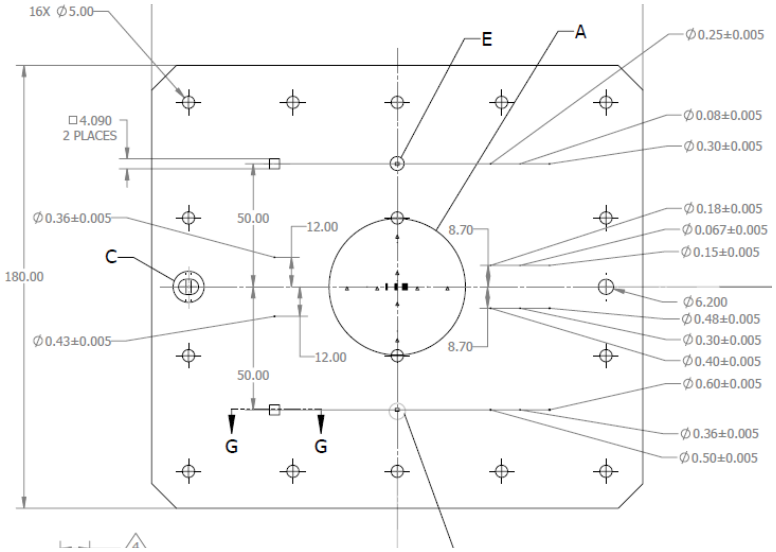

Figure 19. Target plate for straylight data acquisition

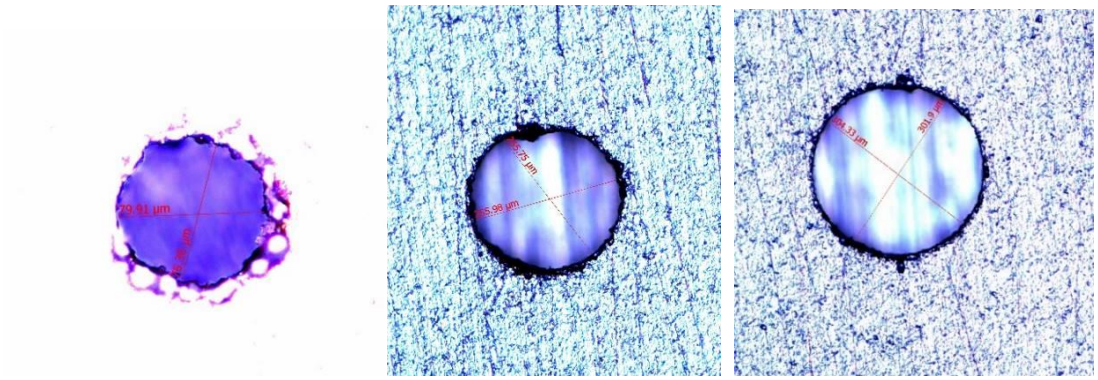

Figure 20. 80µm pinhole (left), 250µm pinhole(middle) and 300µm pinhole (right). Microscope verification of the pinhole dimensions.

The light source used consists of a Xe-arc light source including parabolic mirror and condenser, focusing lens, diaphragm and diffuser (fine-ground glass plate) for intense and uniform illumination on the target area. As the 2-D images are acquired while the target is moving, uniform illumination over a wide area covering the entire motion of the target is required.

The light source produced very high radiance which easily caused saturation of the detector. For some acquisitions the objective was to saturate the captured pinhole image (but not the ghosts), for other acquisitions the objective was to adjust the VSSC signal to approx 1000 DC (just below the saturation level of 1024 DC) in which case an ND filter had to be included in the light source to reduce the light level. Having all detector bands operate at their operational Line-Rate, TDI and VP-gain parameters was desirable but not always possible without saturating the bands with higher sensitivity. Thus, in some cases additional options were used to achieve the desired signal level:

- Adjusting the light source diaphragm aperture, as well as the distance of the light source to the target plate. Using this option required re-evaluation of the uniformity of illumination.
- Varying the VSSC line rate. The line rate is inversely proportional to the integration time, thus increasing the line rate reduces the signal. However, the target scan velocity has to stay compatible with the VSSC line rate, and the linear translator maximum velocity is limited. Therefore, increasing the line rate was a very limited option.
- Adjusting the detector's TDI level (higher TDI ➔ higher signal)
- Increasing/decreasing VSSC Video Processor gain

During some of the measurements, narrow band filters (spectrally identical to VSSC band filters) were included in the light source setup.

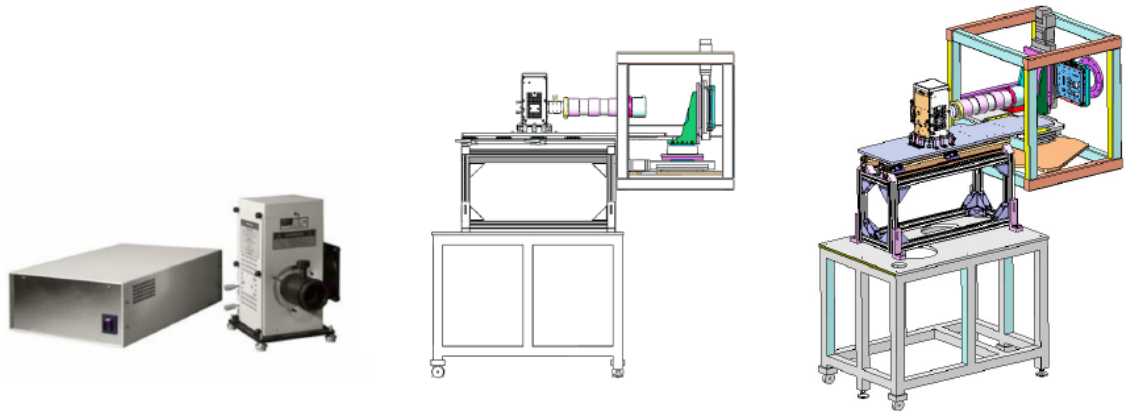

Figure 21. Light Source Xe Lamp (left), Light Source setup versus translators (middle) and target plate (right)

The 2-D image acquisition procedure finally consisted of the following steps:

1. illuminate desired target, close off all other target in the target plate
2. adjust the target plate initial position versus the desired VSSC detector band and pixel location
3. adjust the light level by the means mentioned above to obtain saturation or a signal close to 1000 DC
4. calculate and set the target scan velocity based on the selected VSSC line rate
5. calculate and set the required length of scan based on the scan velocity and target plate initial position
6. verify uniform illumination level over entire path of target motion
7. close off entire collimator focal plane cage to minimize external straylight
8. perform automated scan procedure, capturing 2-D image simultaneously of all detector bands
9. For SL1 data collection repeat the same 2-D image acquisition a number of times, each time after horizontally shifting the initial target position by approx. 20µm, such that the projection on the VSSC focal plane was shifted by approx. 0.5 pixel.

4.2 Local Straylight (SL1) data collection

The following are examples of 2-D images acquired by projecting a 1.64H x 1.23Vmm rectangular target (approx. 40Hx30Vpix in the VSSC focal plane):

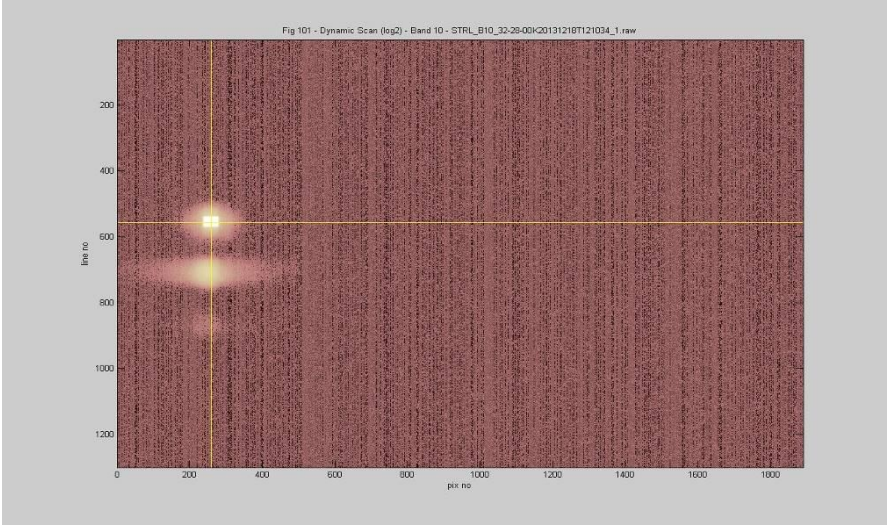

Figure 22. Rectangular target captured on detector band 10 (image size shown approx. 1900Hx1300Vpix)

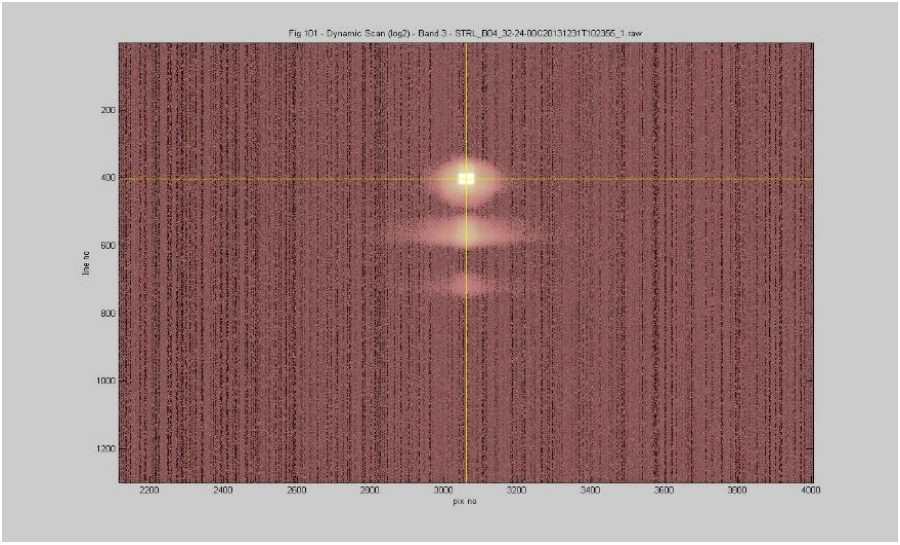

Figure 23. Rectangular target captured on detector band 3 (image size shown approx. 1900Hx1300Vpix)

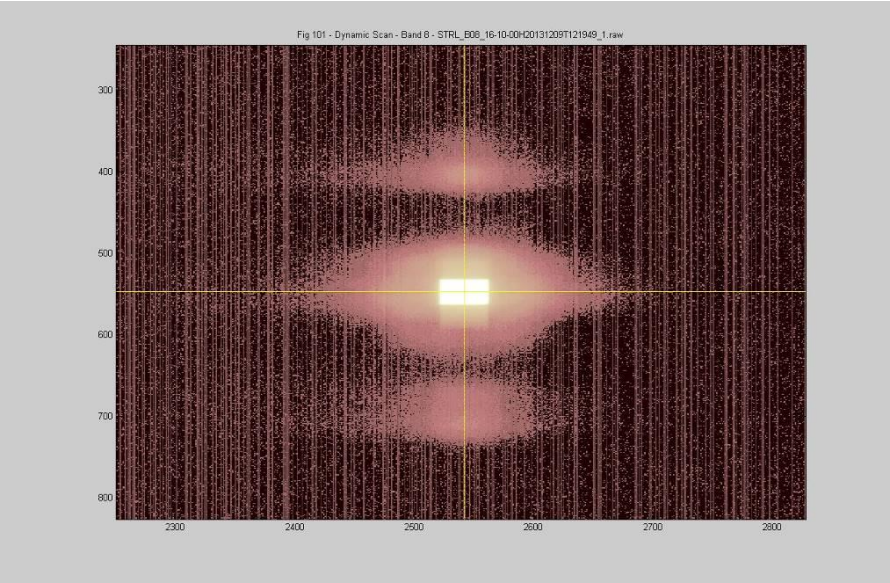

Figure 24. Rectangular target captured on detector band 8 (image size shown approx. 600Hx600Vpix)

4.3 Specific tests to validate assumptions regarding source of crosstalk straylight

The following illustrates a typical 2-D image acquisition of a pinhole in detector band 1 (B1). The image clearly shows crosstalk received from the other bands in the same detector (B2 and B5). The objective of the test is:

- To disprove that the crosstalk originates from outside the detector
- To prove that the crosstalk originates from inside the detector

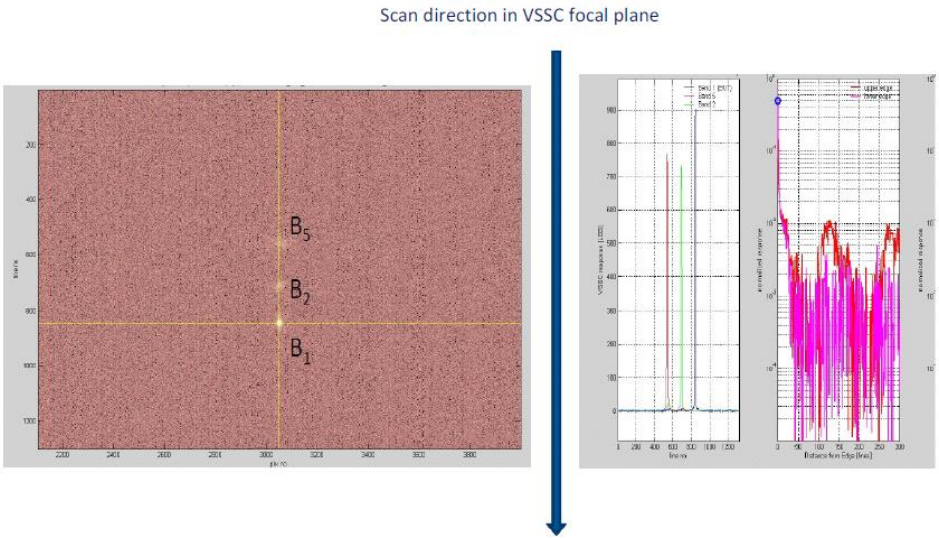

Figure 25. Typical 2-D image acquisition showing crosstalk from other bands in same detector

During the target scan, due to scan direction and separation between the bands, the neighbor bands "see" the target at a different time, namely:

- First B5 "sees" the illuminated target and causes the B5 crosstalk onto B1
- Then B2 "sees" the illuminated target and causes the B2 crosstalk onto B1, while B5 does not any more "see" the target, and B1 does not yet "see" the target
- Finally, B1 captures the illuminated target, while B5 and B2 do not anymore "see" the target

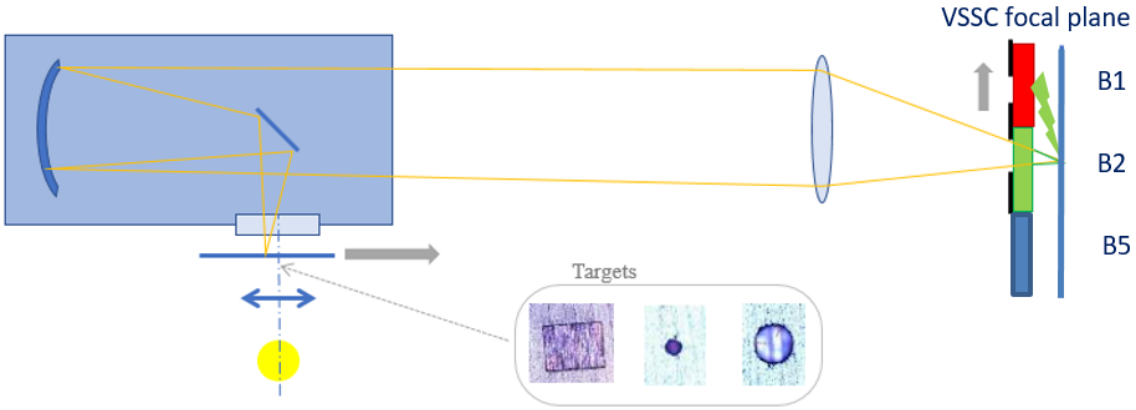

Figure 26. 2-D image acquisition by pushbroom scanning, crosstalk from B2 appears in B1 image

First a target illuminated with white light was projected onto B4. In this case a straylight ghost appeared in both neighbor bands in the same detector (B3 and B6) (see "no filter" image below).
Then a B3 narrowband filter was introduced into the light source, back-illuminating the target with monochromatic light and the same image capture repeated (see "filter B03" image below).
This procedure was repeated with B4 and B6 narrowband filters introduced in the light source (see "filter B04" and "filter B06" images below). The resulting images are shown below.

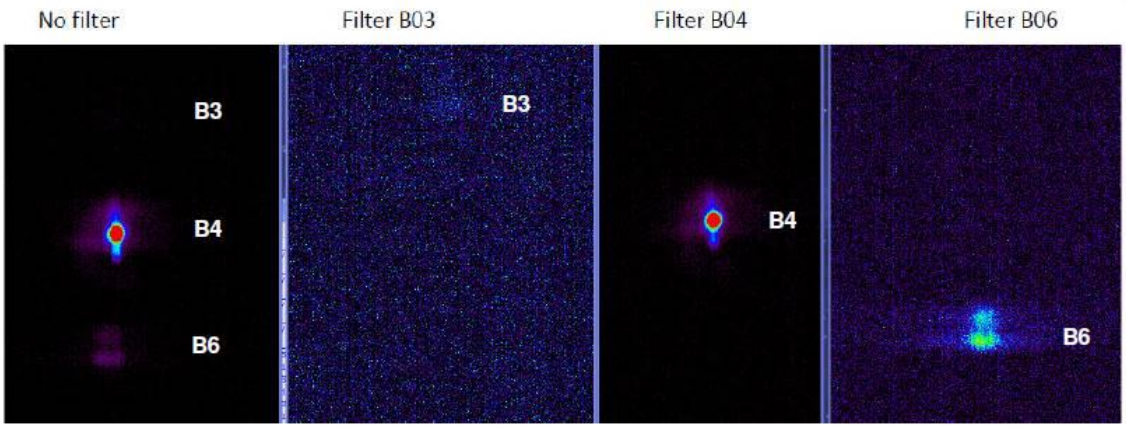

Figure 27. Band 4 images captured when illuminating with white or narrowband filtered light

When the target is illuminated with white light, in addition to the legitimate target image (B4), crosstalk ghosts appear in the B4 band image at locations corresponding to the timing when B3 (top of frame) and B6 (bottom of frame) are "seeing" the illuminated target.
When illuminating with light filtered by a B3 band spectral filter, only the B3 ghost appears in the B4 band image.
When illuminating with light filtered by a B4 band spectral filter, only the B4 legitimate image is observed in the B4 band image.
When illuminating with light filtered by a B6 band spectral filter, only the B6 ghost appears in the B4 band image.

- When illuminating with white light, the relevant spectra of the light can enter each one of the bands.
- When illuminating with B4 filtered light, the "monochromatic" light cannot enter the neighbor bands. The fact that no crosstalk ghosts appear means that there are **no parasitic reflection paths outside** of the detector
- When illuminating with light filtered corresponding to a neighbor's passband, the "monochromatic" light cannot enter B4, hence no target image in B4. The fact that the only crosstalk ghost which appears in B4 corresponds to the timing of that neighbor band, whose spectral passband corresponds to the filtered light, means that there **exist parasitic reflection paths inside** the detector.

The explanation is schematically given in the sketches below assuming a "red" and a "green" filtered band:

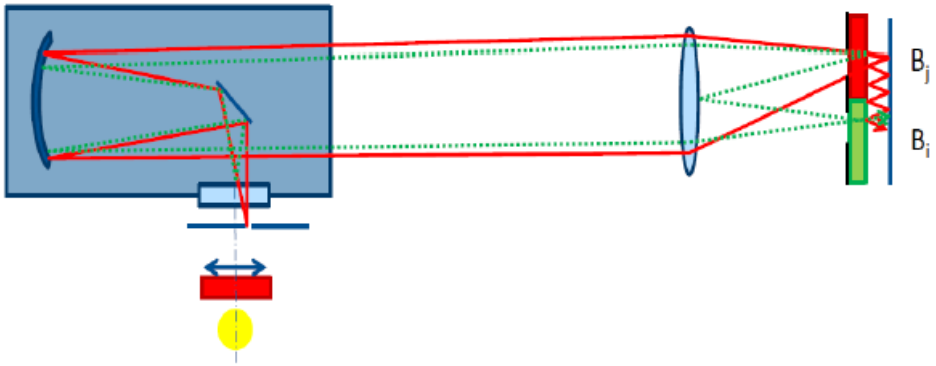

Figure 28. Illuminating band Bj with a red filter

➔ straylight (due to parasitic reflections from optical surfaces outside the detector) cannot reach band Bi

➔ straylight (due to parasitic reflections inside the detector) can reach band Bi

These test results validated conclusively that **crosstalk ghosting between bands occurs within the detector**

4.4 Crosstalk Straylight data collection

The objective for crosstalk straylight data collection is to use the data for estimating and characterizing crosstalk ghost patterns. The tests are performed by illuminating and projecting small targets (pinholes), and measuring the ghost patterns in the non-illuminated areas of the focal plane.

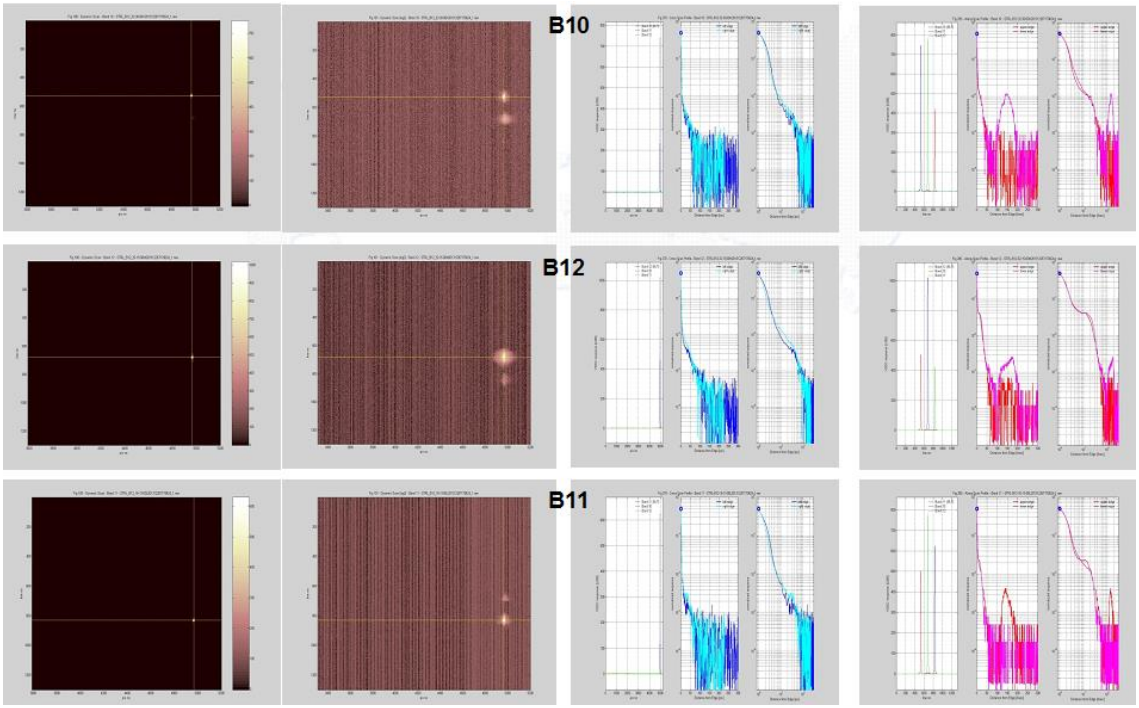

Figure 29. Straylight measurement example – detector 2 – pinhole target

5. MODELING: PRINCIPLES, ASSUMPTIONS AND LIMITATIONS

5.1 Modeling of Local Straylight (SL1)

A Local Straylight (SL1) model is computed as a global system Modulation Transfer Function (MTF) that includes local straylight. This is based on the assumption that the straylight phenomenon can be modelled by a convolution, and that it is slowly variable within the instrument field of view.

The method used is derived from the star-based calibration technique first used for in-flight estimation of the MTF of the PLEIADES satellites, taking advantage of the fact that the stars are motionless, radiometrically known and predictably observable targets [5]. Similarly, for the Venμs camera, where first order aliasing is taken into account since the system MTF at Nyquist spatial frequency (fe) is relatively high (0.15 to 0.2). The unknown is a matrix representing the Fourier Transform (FT) of SL1 straylight, ranging from –fe/2 to +fe/2. If the MTF effects for spatial frequencies higher than fe can be neglected, computing the spatial frequencies up to fe is sufficient. Thus at least 4 measurements are needed, each shifted by a sub-pixel distance, where the shift is modelled by a phase ramp [5]. In order to cancel the effects of measurement noise 10 acquisitions are performed per measurement. Consequently, each measurement then represents the contribution of 4 elements in the equation: the values in both directions (fx, fy) and replicas (fx+fe, fy), (fx, fy+fe), (fx+fe, fy+fe).

Since the useable targets for straylight measurement are much larger than the instrument point spread function, they cannot be considered point sources but must be viewed as disks. The FT of a disk is an Airy function with the first zeroes in the sequence: 1.22, 2.23, 3.24, 4.24, 5.24. A target plate with pinhole targets was specifically prepared with the objective to perform measurements to obtain spatial frequency information around these positions. Using two differently dimensioned pinhole targets, the ratio of pinhole dimensions is chosen in such a way that the first zeroes are as far as possible from one to another: 0.846 is the optimal value for this ratio. The series of measurements is performed with one pinhole and repeated with the second pinhole. After several tests pinhole targets with diameters 250µm and 300µm were used for extended data collection.

Once the MTF is extracted from the measurement data, the target image IMG_Src(i) of spectral band i is deconvoluted with a spatial frequency filter F_i that represents this MTF.

The Fourier transform of the image is computed as the product of 3 terms: The Fourier Transform of the pinhole, computed from its measured diameter, the Fourier Transform of SL1 which includes the system MTF, and the phase ramp associated with the shift between the images computed by correlation between successive images.

5.2 Modeling of Crosstalk straylight (SL2)

To measure the shape of the impulse response of the crosstalk, we observe the pattern generated by high-energy highly saturated pinhole target (80µm diameter) images at the center of the field-of-view. The centering and amplitude of the impulse response is measured from larger targets (30x40 pixels) acquired without saturation. The calculated impulse response is then applied to other patterns for validation and final tuning of the amplitude. The characteristics of the ghost pattern are extrapolated in the whole field-of-view from centering and amplitude laws. Finally, spatial filters are generated, that represent the spreading of crosstalk patterns on a particular band by each of the contributing bands (the 2 other bands of the detector unit).

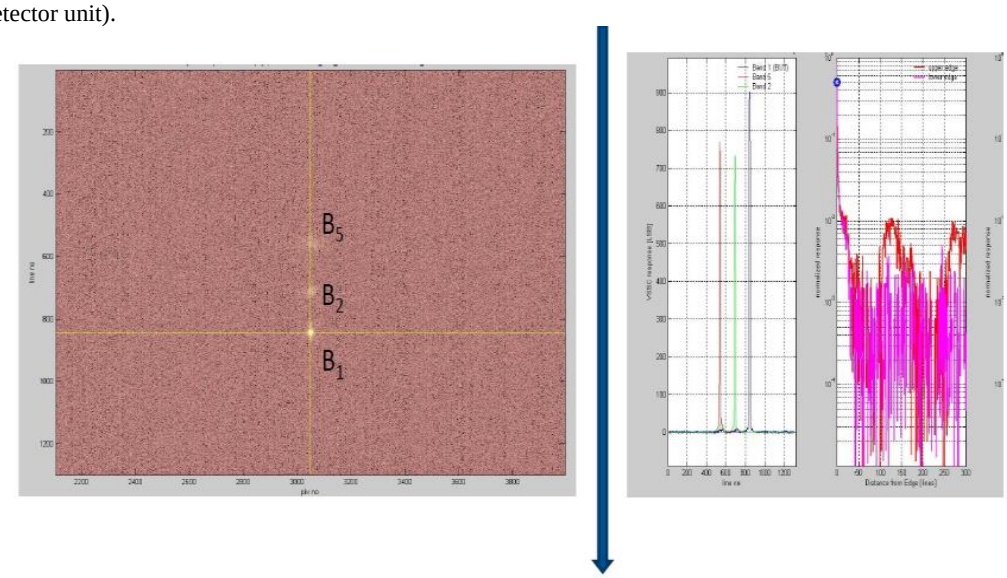

Figure 30. Modeling of crosstalk Straylight - detector 1 – pinhole target

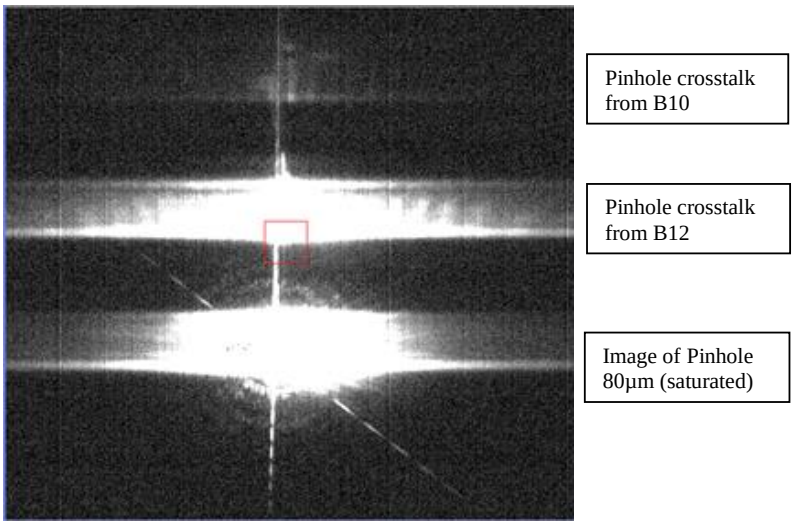

Figure 31. Modeling of crosstalk Straylight – on B11 – saturated pinhole target (radiometric stretch: [0 to 5])

6. IMPLEMENTATION IN LEVEL-1 PROCESSING CHAIN: CONSTRAINTS, TUNING

6.1 Local straylight correction implementation

As defined in §5.1, local Straylight is modelled as a global MTF (MTF_{sys}). The correction is a simple deconvolution of the incoming image by this MTF, in order to reach a 'target MTF' (MTF_{target}). In order to avoid artefacts in the deconvolution, target MTF has been defined to reach 0.1 at Nyquist.
Deconvolution filter F_i in frequency domain is then computed as:

$$F_i = \frac{MTF_{target}}{MTF_{sys,i}}$$

The correction of the images can be written as (i is the index of the band):

$$IMG\_Corr(i) = IMG\_Src(i) \otimes FT(F_i)$$

For most of the bands, the ground measurements showed that the MTF modeling the local Straylight is constant in the swath. For B11 and B12, this is not the case, and the correction is applied on vertical strips, with different deconvolution filters. The corrected strips are then gathered, taking care of the good management of the overlap.

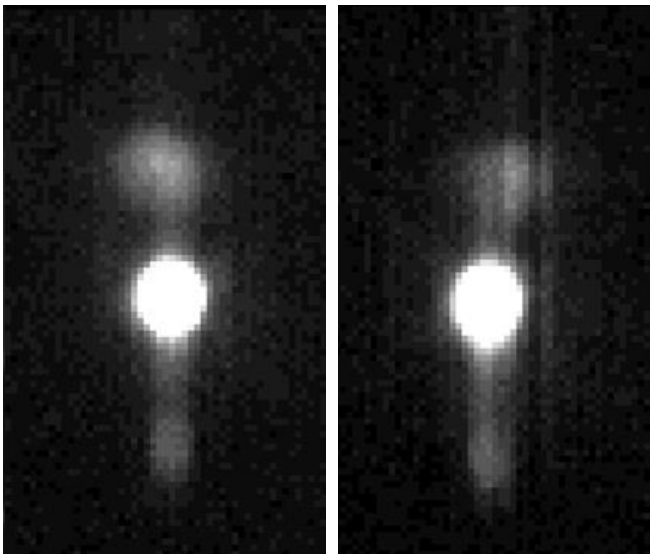

Figure 32. Along swath dependency of local Straylight on B11 (left : col 500, right : col 4700), Straylight generated by a 250µm pinhole

6.2 Crosstalk straylight correction implementation

As seen in §5.2, the crosstalk Straylight is modelled by :

- the spatial impulse response ($G_{j->i}$), computed at center of the swath
- The centering law: due to angular effects, the centering of the filter is depending on the location in the swath (shift is of about 3.8 pixels each 1000 column). The impulse response has to be translated, depending on the column (function 'trans (filter, column)')
- The amplitude of the crosstalk, is also depending on the location in the swath. The impulse response has to be multiplied by this amplitude factor (A), depending on the column.

The crosstalk signals for all contributing bands j of the same tri-detector are then substracted from the image of band i.

$$IMG_{Corr(i)} = IMG_{Src(i)} - \sum_{j} IMG_{Src(j)} \otimes (trans(G_{j\rightarrow i} * A_{j\rightarrow i,col}, col)$$

For an efficient implementation of the correction, it has been decided to split the swath into vertical strips. In each strip, the amplitude and the translation is considered unchanged. A drawback of this implementation lies in the difficulty to manage the possible discontinuities between strips on overlap regions, mainly on uniform areas, when amplitude factor strongly varies in the swath.

7. IN-FLIGHT PERFORMANCE ESTIMATION

7.1 Acquisitions used for performance assessment and tuning of parameters

Moon acquisitions provide valuable information for analysing the performance of straylight correction, since the reference signal can be characterized with precision: the background is composed of total darkness and the geometry of the image is known. 15 moon images from September 27 to December 9, 2017 are used.

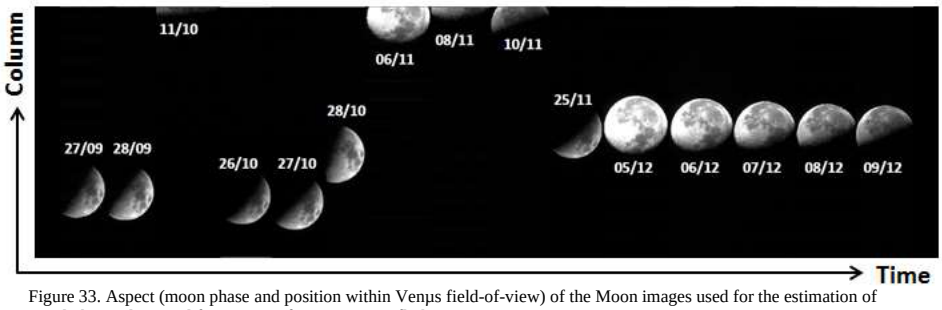

Figure 33. Aspect (moon phase and position within Venμs field-of-view) of the Moon images used for the estimation of straylight residues, and fine tuning of parameters in flight.

For both types of straylight, the performance of the applied correction may be evaluated by computing a signal-to-noise ratio (SNR), considering firstly the straylight pattern as noise (raw performance), and secondly the residue after applying the correction as noise (final performance). The SNR is estimated for typical cases of the Venμs mission, which are defined as typical sharp landscape transitions from bare soil to vegetation. The performance is assessed by computing an SNR at a given distance from these L_{veg} to L_{soil} transitions, simulated by the L_{dark} to L_{moon} transitions visible in moon images, before and after applying the straylight corrections. The moon acquisition dated December 5, 2017 is used as a reference, as it represents the moon acquisition with maximum signal obtained during IOT.

Moreover, the drawing of averaged profiles of Dark/Moon transitions has helped the fine tuning of the correction parameters.

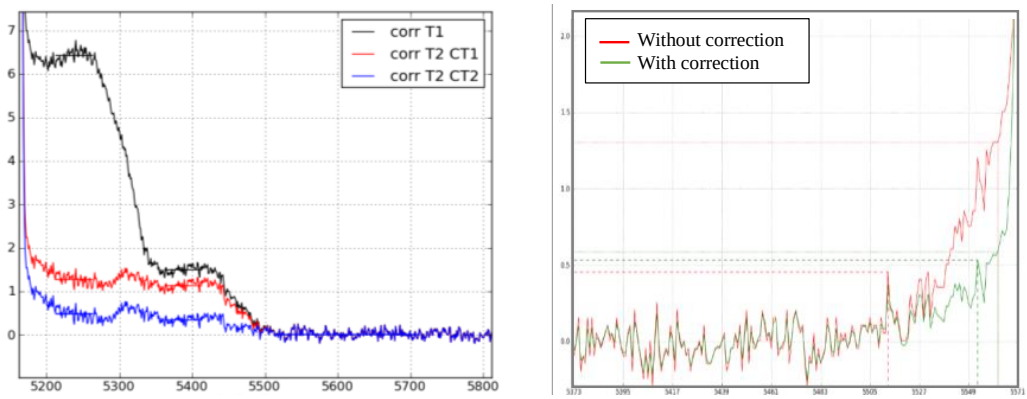

Figure 34. profiles on Moon transition for the fine tuning and assessment of the Straylight correction on B3
- left : profile along columns for crosstalk (below the Moon)
- right : profile along columns for local straylight (left side of the Moon)

7.2 Local straylight estimation and correction performance

The straylight correction performance is estimated from the signal measured in the dark part of the image, at a distance of 10 native pixels from the transition to the bright part (moon), on the 4 observable geometries of directions of transitions (top, bottom, left and right) whenever the local straylight is observable on the dark background, i.e. when no crosstalk straylight is affecting the transition. The computation is performed on raw images, and then on corrected images. From this, the correction performance can be assessed in terms of reduction of the local straylight which is considered as noise. On average, the level of the SL1 straylight signal at 10 pixels from the transition is reduced by 50%.

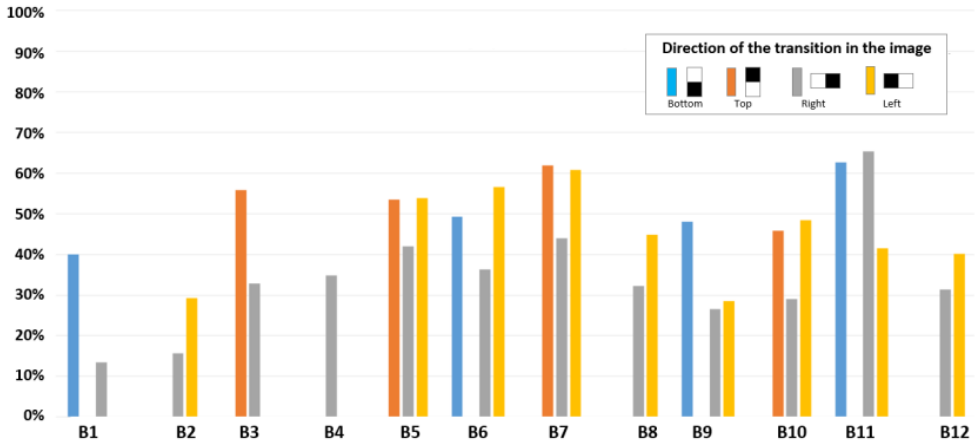

Figure 35. Estimated performance of the local ghost correction: reduction of noise at 10 pixels from the transition

7.3 Crosstalk straylight estimation and correction performance

In a similar way for each identified crosstalk ghost in the moon images, after removing the background signal we can estimate the crosstalk level from the uncorrected raw images and then from the corrected images.

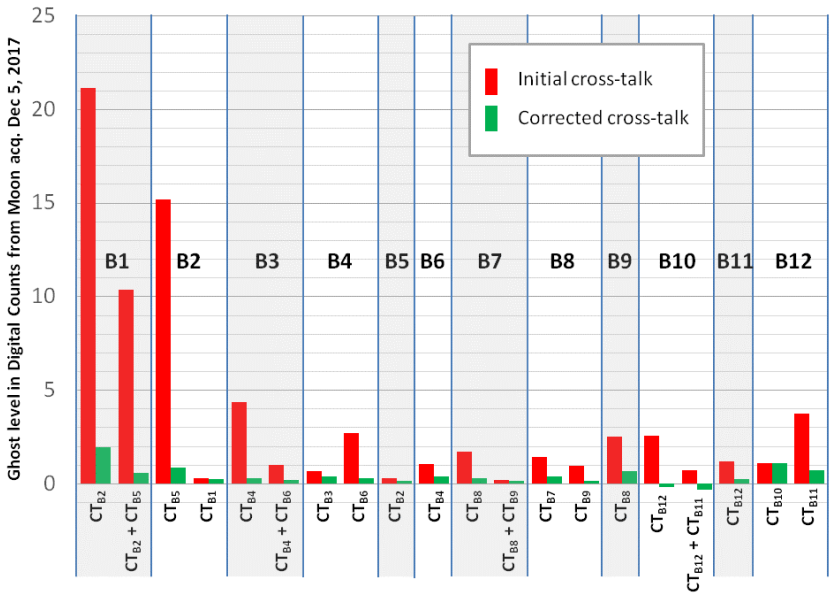

Figure 36. Crosstalk Ghost levels from uncorrected L0 images, and from L0 images after applying the corrections

If we except the crosstalk ghost from B2 to B1, which is partly generated by the overlapping spectral responses of the 2 bands, the residue after correction from SL2 straylight is below 1 DC.

This very low residue confirms the accuracy of the model as well as the linearity of the detectors, as the results are computed from a relatively low radiance moon image, whereas the correction model was parameterized with ground measurements based on Lmax illumination levels as defined per spectral band.

7.4 Visual analysis of the corrected images

A visual analysis of images of typical landscapes, on which the different types of straylight were observed, was performed during the IOT.

On the following sample images, the dynamics have been adapted to accentuate the straylight phenomena. In order to show the effect of the implemented straylight correction, identical dynamics have been used to display the raw image (left) and the image after correction (right).

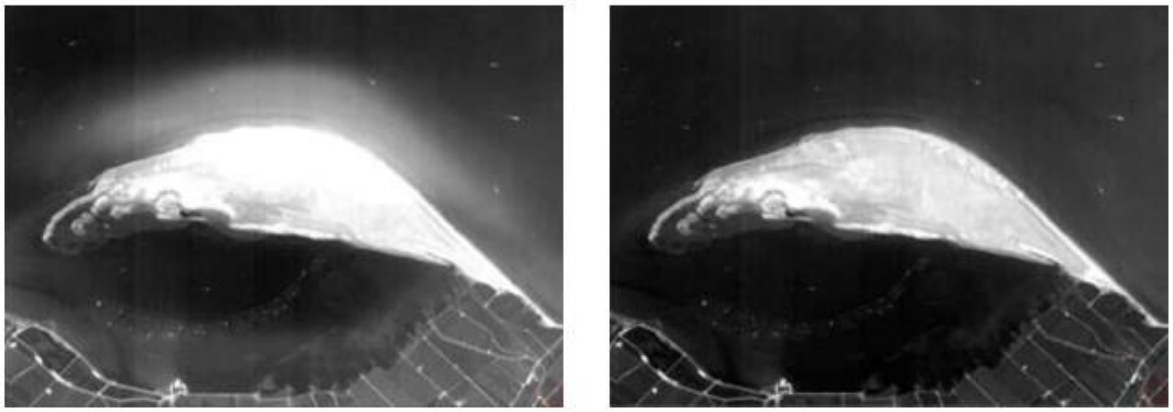

Figure 37. B1 image of the Ebro delta, Sept. 8, 2017

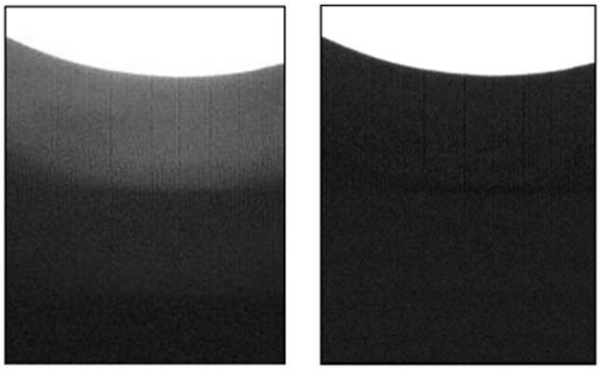

Figure 38. B3 Moon transition, Dec 5, 2017

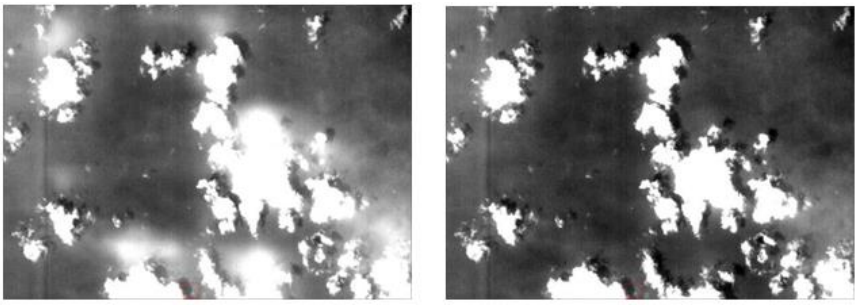

Figure 39. B2 image over North Atlantic, Aug. 18, 2017

8. CONCLUSIONS

The necessary tuning of the correction model during the in-orbit test phase was minor, which shows that the global in-flight performances are in line with the ground tests. It shows also that the observed phenomena are stable in time. Ultimately, it confirms the validity of the assumptions and prerequisites made for the modeling.

Eventually, Venμs was successfully radiometrically calibrated [3], although the process was very challenging. Thanks to an innovative modeling of the phenomenon, associated to a meticulous ground measurement campaign and a specific effort on the implementation in the production chain, the consequences of the issue were mitigated and the post processed Venμs product matches the scientific requirements, except for some difficult sites.

The radiometric performance is good for bands B3 to B11. As anticipated, it is not accurate enough for the blue bands B1 and B2. It will be updated soon for water vapour band B12. A reprocessing is scheduled at the end of 2018 with an updated configuration, bringing an enhanced geometric performance [4] and a fine radiometric calibration for B12.

Level-2 time series and level-3 products are now being produced and freely available to users via the THEIA land data center **www.theia-land.fr**.

9. ACKNOWLEDGEMENTS

The authors wish to thank ELOP / ELBIT-Systems for their support in the extensive ground characterization of the straylight phenomena, CNES radiometric Image Quality and instrument teams, and the Magellium team for their work in the implementation and fine tuning of the straylight correction algorithm.

REFERENCES

[1] Pierric Ferrier, Philippe Crebassol, Gérard Dedieu, Olivier Hagolle, Aimé Meygret, Francesc Tinto, Yoram Yaniv, Jakob Herscovitz, "Venμs (Vegetation and environment monitoring on a new micro satellite)", 2010 IEEE International Geoscience and Remote Sensing Symposium, Honolulu, HI, pp. 3736-3739. doi: 10.1109/IGARSS.2010.5652087 (2010)

[2] Gérard Dedieu, Arnon Karnieli, Olivier Hagolle, Hervé Jeanjean, François Cabot, Pierric Ferrier, Yoram Yaniv, “Venμs: a joint French Israeli Earth observation mission with high spatial and temporal resolution capabilities”, RAQRS II conference (2006)

[3] Philippe Gamet, Arthur Dick, Sébastien Marcq, Olivier Hagolle, Jean-Louis Raynaud, Philippe Crébassol, Emmanuel Hillairet, Silvia Juglea, Jean-Pascal Burochin, “Venμs in orbit radiometric calibration”, SPIE Remote Sensing Berlin (2018)

[4] Renaud Binet, Françoise De Lussy, Florie Languille, Amandine Rolland, Jean-Louis Raynaud, Bernard Specht, “Venμs geometric image quality commissioning”, SPIE Remote Sensing Berlin (2018)

[5] Sébastien Fourest, Laurent Lebegue, “Star-based calibration techniques for PLEIADES-HR satellites”, CALCON 2009 proceedings (2009)